© 2022. Published by The Company of Biologists Ltd | Journal of Cell Science (2022) 135, jcs259145. doi:10.1242/jcs.259145

RESEARCH ARTICLE

SPECIAL ISSUE: CELL BIOLOGY OF LIPIDS

Dishevelled coordinates phosphoinositide kinases PI4KIIIα and PIP5KIγ for efficient PtdInsP_2 synthesis

Lizbeth de la Cruz, Raul Riquelme, Oscar Vivas, Andres Barria and Jill B. Jensen*

ABSTRACT

Phosphatidylinositol(4,5)-bisphosphate (PtdInsP_2) is an important modulator of many cellular processes, and its abundance in the plasma membrane is closely regulated. We examined the hypothesis that members of the Dishevelled scaffolding protein family can bind the lipid kinases phosphatidylinositol 4-kinase (PI4K) and phosphatidylinositol 4-phosphate 5-kinase (PIP5K), facilitating synthesis of PtdInsP_2 directly from phosphatidylinositol. We used several assays for PtdInsP_2 to examine the cooperative function of phosphoinositide kinases and the Dishevelled protein Dvl3 in the context of two receptor signaling cascades. Simultaneous overexpression of PI4KIIIα (also known as PI4KA) and PIP5KIγ (also known as PIP5K1C) had a synergistic effect on PtdInsP_2 synthesis that was recapitulated by overexpression of Dvl3. Increasing the activity of Dvl3 by overexpression increased resting plasma membrane PtdInsP_2. Knockdown of Dvl3 reduced resting plasma membrane PtdInsP_2 and slowed PtdInsP_2 resynthesis following receptor activation. We confirm that Dvl3 promotes coupling of PI4KIIIα and PIP5KIγ and show that this interaction is essential for efficient resynthesis of PtdInsP_2 following receptor activation.

KEY WORDS: Dishevelled, Dvl3, PtdInsP_2, Ror2, Wnt, Kinase, Phosphoinositide

INTRODUCTION

This paper investigates in living cells the organization and cooperative action of phosphoinositide kinases and Dishevelled (Dvl) proteins, a family of scaffolding proteins that organize effectors of Wnt signaling pathways (Sharma et al., 2018). Phosphoinositides are minority membrane lipids with important functions in cellular signaling. The heterogeneous distribution of phosphoinositides gives each cellular membrane a distinct lipid signature, and this distribution is kept in homeostasis by regulation of lipid kinases and phosphatases. Phosphatidylinositol (PtdIns) can be phosphorylated on the 3-, 4-, or 5-hydroxyl positions of its myo-inositol ring to generate seven species of phosphoinositides, including phosphatidylinositol(4,5)-bisphosphate (PtdInsP_2), which resides on the inner, cytoplasmic leaflet of the plasma membrane. PtdInsP_2 is an important signaling molecule with diverse cellular functions including regulating ion channels and transporters, remodeling the cytoskeleton, and regulating vesicle movement and fusion (Balla, 2013; Mandal, 2020).

Our focus is the generation of PtdInsP_2 from PtdIns via phosphorylation by phosphatidylinositol 4-kinase (PI4K) and phosphatidylinositol 4-phosphate 5-kinase (PIP5K). The synthesis of PtdInsP_2 from PtdIns is typically considered as two sequential and physically separate reactions catalyzed by PI4K and PIP5K (Fig. 1A, top). A recent kinetic model of phosphoinositide dynamics (Olivença et al., 2018) found it necessary to postulate direct transformation of PtdIns into PtdInsP_2 to match experimental rates of PtdInsP_2 production, especially under conditions of low phosphatidylinositol (4)-phosphate (PtdIns$P$). Previous evidence for a ternary complex that includes both kinases and a scaffolding protein (Fig. 1A, bottom) comes from co-immunoprecipitation experiments showing physical association amongst PI4K type IIα (also known as PI4K2A), PIP5K and a Dvl scaffolding protein during Wnt signaling (Qin et al., 2009). We assessed the degree to which a different type of PI4K and PIP5KIγ (also known as PIP5K1C) associate and the functional consequences of this partnership in the context of two receptor signaling cascades.

Here, we compared signaling from two types of receptors. The M_1 muscarinic acetylcholine receptor (CHRM1, referred to here as M_1 receptor) couples to Gαq and phospholipase C beta (PLCβ) to hydrolyze PtdInsP_2 to inositol (1,4,5)-trisphosphate (InsP_3) and diacylglycerol, leading to several downstream events including an increase in Ca^{2+} concentration, membrane depolarization and regulation of several ion channels (Hille et al., 2015). The Ror2 receptor is a tyrosine kinase-like non-canonical Wnt receptor known to associate with Dvl proteins (Nishita et al., 2010; Witte et al., 2010). The early signaling events initiated by Ror2 are less well defined. In neurons, activation of Ror2 leads to an increase in intracellular Ca^{2+}, membrane depolarization and increased trafficking of NMDA receptors (Cerpa et al., 2011; 2015; McQuate et al., 2017). Dvl proteins regulate the cytoskeleton, modify synaptic activity and shuttle to the nucleus (Ahmad-Annuar et al., 2006; Castro-Piedras et al., 2021; Sharma et al., 2018; Sheldahl et al., 2003). Genetic mutations in *DVL1*, *DVL3*, *ROR2* or *WNT5A* cause impaired development, particularly affecting the skeleton, classified as Robinow syndrome (White et al., 2015, 2016, 2018). We tested the role of the Dvl protein Dvl3 in PtdInsP_2 metabolism downstream of both receptors and compared it to the role of phosphoinositide kinases.

The localization and regulatory context of phosphoinositide kinases is becoming apparent through structural and functional studies. The substrate of PI4K, PtdIns, is abundant on the endoplasmic reticulum, where colocalization with the PtdIns$P$ 4-phosphatase Sac1 (also known as SACM1L) prevents the accumulation of PtdIns$P$. PtdIns is transported from the endoplasmic reticulum to the plasma membrane by PtdIns transfer proteins. PI4KIIIα (also known as PI4KA) – which is cytosolic when expressed alone – is anchored to the plasma membrane by

Department of Physiology and Biophysics, University of Washington School of Medicine, Seattle, WA 98195-7290, USA.

*Author for correspondence (jbodily@uw.edu)

L.d.l.C., 0000-0003-1243-2276; O.V., 0000-0002-0964-385X; A.B., 0000-0001-7724-0043; J.B.J., 0000-0002-3527-0911

Handling Editor: James Olzmann
Received 14 July 2021; Accepted 14 December 2021

Journal of Cell Science (2022) 135, jcs259145. doi:10.1242/jcs.259145

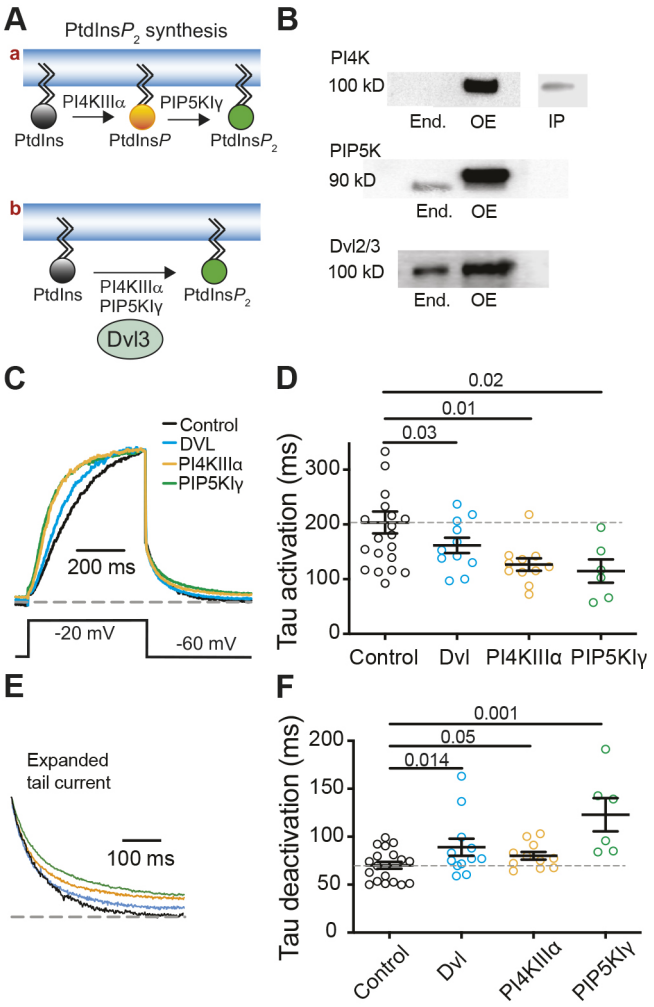

Fig. 1. Overexpression of Dvl3 increases baseline PtdInsP_2. (A) Schematic representation of PtdInsP_2 synthesis as sequential phosphorylation by PI4KIIIα and PIP5KIγ (top) or as coupled and concerted activity of the two phosphoinositide kinases (bottom). (B) Immunoblots showing expression of PI4K, PIP5K, or Dvl2 and Dvl3 (Dvl2/3) in untransfected tsA-201 cells (End.) and in cells overexpressing (OE) PI4K (top), PIP5K (middle) or Dvl3 (bottom). Note that recombinant proteins are tagged with fluorophore; therefore, they run at higher molecular weights (indicated in kilodaltons, kD). Endogenous PI4KIIIα was detected following immunoprecipitation (IP). Blots are representative of six experiments. (C) Normalized voltage-clamp current traces from tsA-201 cells overexpressing KCNQ2 and KCNQ3 channel subunits (control, black) and Dvl3 (DVL, blue), PI4KIIIα–GFP (orange) or PIP5KIγ–GFP (green). (D) The exponential time constant (tau) of KCNQ2/3 activation for conditions as in A. Mean±s.e.m. tau of activation: 204±20 ms (control, *n*=21), 162±14 ms (Dvl3, *n*=11), 126.7±11 ms (PI4KIIIα, *n*=11), 115±21 ms (PIP5KIγ, *n*=6). (E) Normalized expanded tail current from C to show deactivation. (F) Exponential time constants of KCNQ2/3 deactivation. Mean±s.e.m. tau of deactivation: 70±4 ms (control, *n*=21), 89±9 ms (Dvl3, *n*=11), 80±4 ms (PI4KIIIα, *n*=11), 123±17 ms (PIP5KIγ, *n*=6). Dashed lines in D and F mark the mean control value. *P*-values are shown for the comparisons indicated by horizontal bars (ANOVA with Dunnett's multiple comparison test).

cognate proteins, several pairs of which are sufficient plasma membrane tethers: EFR3A/B and TTC7A/B, EFR3A/B and TMEM150A, TTC7A/B and FAM126A (Chung et al., 2015; Lees et al., 2017; Nakatsu et al., 2012). PIP5K localizes to the plasma membrane, and the catalytic activity of PIP5K1A is enhanced by binding the DIX domain of Dvl1 (Hu et al., 2015). We build on this context to show how these proteins work together in living cells. In this paper, we show that Dvl3 organizes PI4K and PIP5K for enzymatic synergy in synthesizing PtdInsP_2, that this mechanism is essential for timely PtdInsP_2 resynthesis following M_1 receptor activation, and that Ror2 increases PtdInsP_2, likely via interaction with Dvl3 and PIP5K.

RESULTS

Dvl3 increases baseline PtdInsP_2

This study tests the hypothesis that Dvl proteins organize PI4K and PIP5K to facilitate synthesis of PtdInsP_2 (Fig. 1A). Immunoblots for PI4KIIIα, PIP5KIγ, and Dvl2 and Dvl3 confirmed that these proteins are expressed endogenously in untransfected human tsA-201 cells and that overexpression increases their levels as expected (Fig. 1B). Endogenous PI4KIIIα was imperceptible in whole-cell lysates but could be detected following immunoprecipitation with an anti-PI4K antibody.

We assessed PtdInsP_2 levels by measuring potassium currents upon overexpression of KCNQ2 and KCNQ3 (referred to hereafter as KCNQ2/3). Due to their high sensitivity to plasma membrane PtdInsP_2 levels (Li et al., 2005), KCNQ2/3 potassium channels (M current) are specific real-time indicators of plasma membrane PtdInsP_2 in living cells. KCNQ2/3 currents are virtually eliminated by strong activation of PLCβ and subsequent depletion of PtdInsP_2 (Horowitz et al., 2005), whereas increased levels of PtdInsP_2 are correlated with faster activation gating and slower deactivation of the channel (Dai et al., 2016). Changes to baseline PtdInsP_2 levels could be ascertained from activation and deactivation kinetics of KCNQ2/3 currents elicited by a depolarizing pulse to −20 mV. Overexpression of the scaffolding protein Dvl3 accelerated activation gating and slowed deactivation compared to control cells, indicating an increase in steady-state levels of plasma membrane PtdInsP_2 (Fig. 1C–F, blue traces). As expected, overexpressing either PI4KIIIα or PIP5KIγ also accelerated activation and slowed deactivation (Fig. 1C–F, orange and green traces, respectively).

Dvl3 accelerates PtdInsP_2 resynthesis

To establish the cellular consequences of Dvl proteins on PtdInsP_2, we studied the effects of Dvl3 overexpression on the kinetics of PtdInsP_2 depletion and resynthesis in the dynamic environment of receptor activation. Activation of Gq-coupled receptors such as the M_1 receptor activates PLCβ, causing hydrolysis of PtdInsP_2 (Horowitz et al., 2005). We assessed PtdInsP_2 localization using PH-PLCδ1, a fluorophore-tagged probe that serves as a specific visual indicator of PtdInsP_2 (Varnai et al., 2006). In control cells, PH-PLCδ1 accumulated primarily at the plasma membrane, as expected, and transiently translocated to the cytosol upon activation of the M_1 receptor, reflecting hydrolysis of PtdInsP_2 by PLCβ (Fig. 2A–C; control in A, black trace in B and C). Overexpressing Dvl3 reduced the baseline cytosolic intensity of PH-PLCδ1 (Fig. 2B, blue trace), indicating increased resting plasma membrane PtdInsP_2. When M_1 receptors were activated in cells overexpressing Dvl3, much of the PH-PLCδ1 was retained at the plasma membrane; translocation to the cytosol was reduced (Fig. 2G), and the probe returned to its baseline distribution much faster than in control cells (Fig. 2H). The reduced initial translocation to the cytosol and the faster recovery of the probe to the plasma membrane suggest larger resting pools and accelerated synthesis of PtdInsP_2 in the presence of overexpressed Dvl3.

PI4K and PIP5K work synergistically to generate PtdInsP_2

To understand the relationship of Dishevelled proteins with PI4KIIIα and PIP5KIγ, we compared the overexpression of Dvl3 with overexpression of the phosphoinositide kinases alone or

Journal of Cell Science (2022) 135, jcs259145. doi:10.1242/jcs.259145

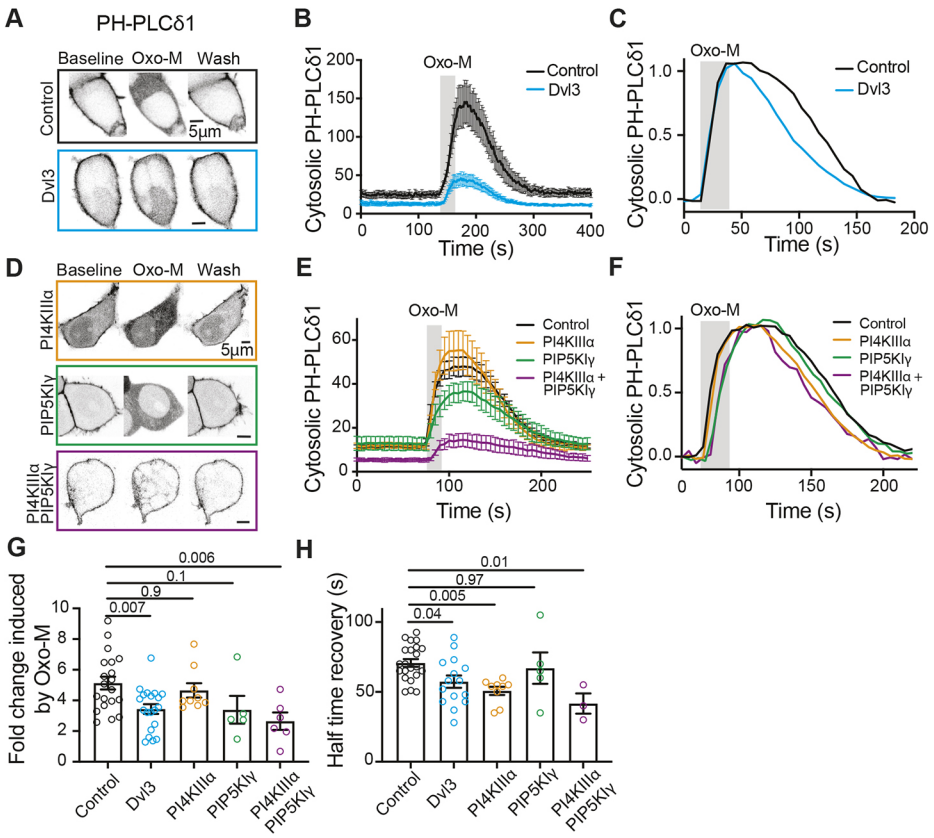

Fig. 2. Overexpression of Dvl3 accelerates PtdInsP_2 resynthesis, mimicking overexpression of PI4KIIIα and PIP5KIγ. (A) Contrast-inverted Airyscan confocal micrographs of tsA-201cells overexpressing M_1 receptor and the PtdInsP_2 probe PH-PLCδ1–RFP alone (control) or with co-expression of Dvl3–YFP (blue). PH-PLCδ1 localizes to the plasma membrane at rest and relocates to the cytoplasm when Oxo-M (1 μM) activates M_1 muscarinic receptors, depleting PtdInsP_2. After removal of Oxo-M (wash), PH-PLCδ1 returns to the plasma membrane, indicating resynthesis of PtdInsP_2. (B) Time course of cytosolic intensity of PH-PLCδ1 in control and Dvl3-overexpressing cells as in A. Note that an increase in cytosolic PH-PLCδ1 indicates a decrease in plasma membrane PtdInsP_2. Mean±s.e.m. baseline cytosolic PH-PLCδ1: 24±4 (control, *n*=11), 12±2 (Dvl3, *n*=20). (C) Same mean data as in B, normalized for comparison of kinetics. (D) Contrast-inverted Airyscan confocal micrographs from tsA-201 cells overexpressing M_1 receptor, PH-PLCδ1–RFP, and either PI4KIIIα–GFP (orange), PIP5KIγ–GFP (green) or PI4KIIIα–GFP and PIP5KIγ–CFP together (purple), treated as in A. (E) Time course of cytosolic intensity of PH-PLCδ1 in kinase-overexpressing cells as in D. Control, tsA-201 cells overexpressing M_1 receptors and PH-PLCδ1–RFP. Mean±s.e.m. baseline cytosolic PH-PLCδ1: 11±1 (control, *n*=12), 12±1 (PI4KIIIα, *n*=9), 13±3 (PIP5KIγ, *n*=5), 6±1 (PI4KIIIα+PIP5KIγ, *n*=6). (F) Same mean data as in E, normalized for comparison of kinetics. (G) Fold change in peak cytosolic intensity of PH-PLCδ1 following activation of M_1 receptors in B and E. Mean±s.e.m. fold change: 5.2±0.4 (control, *n*=20), 3.4±0.3 (Dvl3, *n*=20), 4.6±0.5 (PI4KIIIα, *n*=9), 3.3±0.9 (PIP5KIγ, *n*=5), 2.6±0.56 (PI4KIIIα+PIP5KIγ, *n*=6). (H) The half time for recovery of cytosolic PH-PLCδ1–RFP following M_1 receptor activation in B and E. Mean±s.e.m. half time of recovery: 71±3 s (control, *n*=20), 57±4 s (Dvl3, *n*=20), 51±3 s (PI4KIIIα, *n*=9), 67±11 s (PIP5KIγ, *n*=5), 42±7 s (PI4KIIIα+PIP5KIγ, *n*=3). *P*-values are shown for the comparisons indicated by horizontal bars (ANOVA with Dunnett's multiple comparison test).

together. We found that neither PI4KIIIα nor PIP5KIγ overexpressed alone changed the baseline cytosolic distribution of PH-PLCδ1, but that in combination they increased resting plasma membrane PtdInsP_2, as reflected by decreased baseline cytosolic intensity of PH-PLCδ1 (Fig. 2E, purple trace). Activation of M_1 receptors in cells overexpressing either PI4KIIIα or PIP5KIγ depleted PtdInsP_2 from the plasma membrane, seen as a transient increase in cytosolic PH-PLCδ1 (Fig. 2D,E). Overexpression of either kinase altered the kinetics of PH-PLCδ1 movement in response to activation of M_1 receptors, with PIP5KIγ delaying the release of PH-PLCδ1 from the plasma membrane during M_1 receptor activation and PI4KIIIα accelerating the return of PH-PLCδ1 to the plasma membrane during resynthesis of PtdInsP_2 (Fig. 2H). When both kinases were co-expressed, translocation of PH-PLCδ1 to the cytosol was suppressed by 62%, similar to the effect of overexpression of Dvl3 (Fig. 2G). In the few cells with evident translocation of PH-PLCδ1, kinetic rates matched those for overexpression of PIP5KIγ during PtdInsP_2 hydrolysis and those for PI4KIIIα during PtdInsP_2 resynthesis (Fig. 2F,H). These data suggest that overexpression of Dvl3 recapitulates the co-overexpression of PI4KIIIα and PIP5KIγ and support the idea that Dishevelled proteins coordinate PI4KIIIα and PIP5KIγ to act synergistically to synthesize PtdInsP_2. Our data also suggest that PI4KIIIα is rate limiting in PtdInsP_2 synthesis, in agreement with our previous work (Falkenburger et al., 2010).

Interpretation of these results must be tempered with acknowledgement of the constraints of the probe used. Although PH-PLCδ1 allows us to observe net changes in plasma membrane PtdInsP_2, it may not be a fully linear indicator of PtdInsP_2 (Myeong et al., 2020). PH-PLCδ1 mobility is likely saturated at high PtdInsP_2 levels (such that no further movement to the plasma membrane is possible even with increasing PtdInsP_2), for instance when Dvl3 is overexpressed or both kinases are overexpressed together.

PI4K, PIP5K and Dvl3 mutually reinforce localization to the plasma membrane

Since PI4KIIIα and PIP5KIγ appear to work synergistically to synthesize PtdInsP_2 and overexpressed Dvl3 recapitulates the effects of PI4K and PIP5K co-expression, we hypothesized that these proteins might colocalize. The localization of PI4K, PIP5K and Dvl3 was probed using high-resolution confocal microscopy

Journal of Cell Science (2022) 135, jcs259145. doi:10.1242/jcs.259145

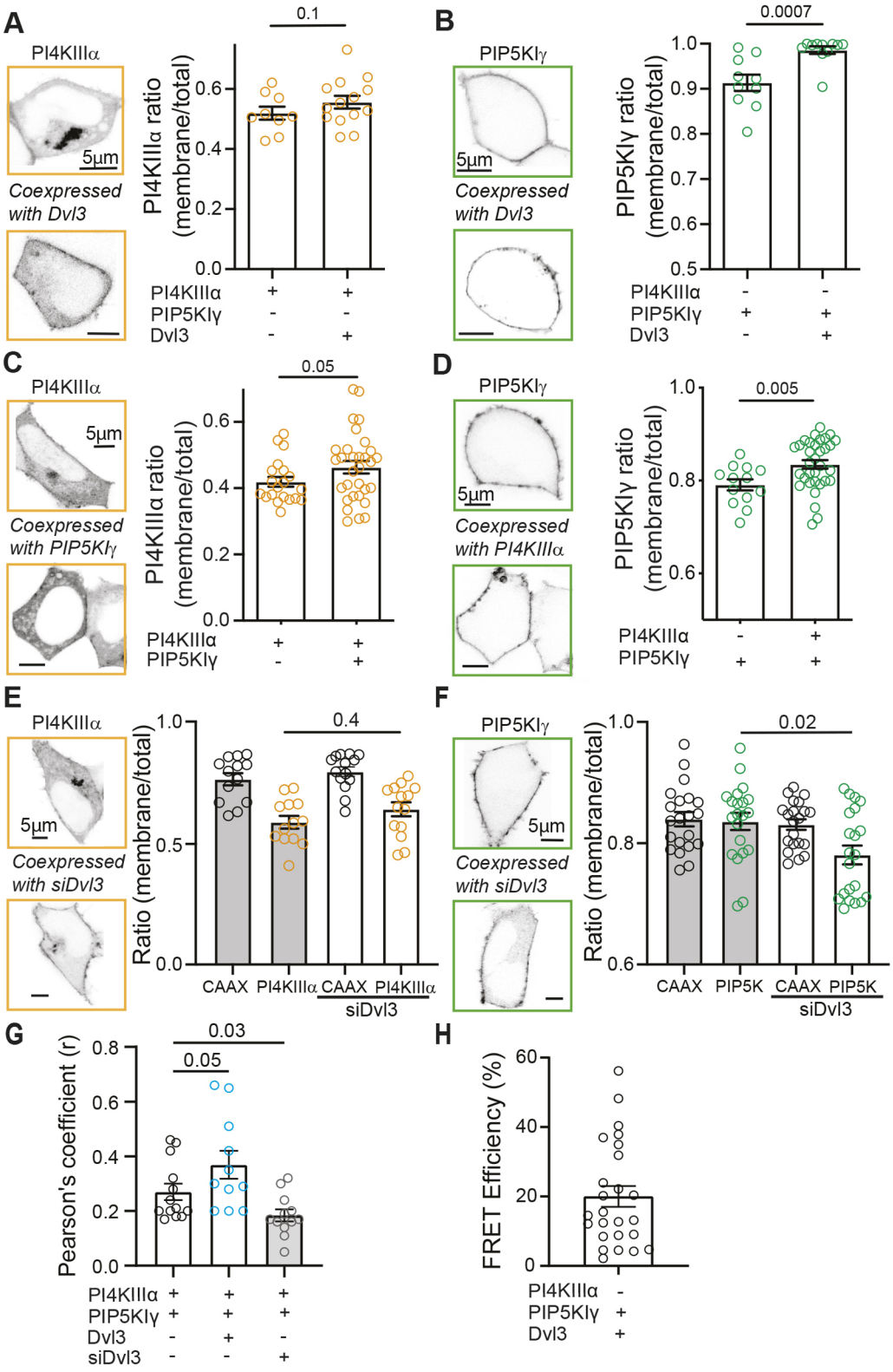

Fig. 3. See next page for legend.

and fluorescence resonance energy transfer (FRET). Overexpressed PI4KIIIα was found in the cytosol, plasma membrane and a Golgi-like structure (Fig. 3A), whereas PIP5KIγ was localized primarily in the plasma membrane (Fig. 3B). To facilitate plasma membrane docking of PI4KIIIα, throughout this paper this kinase was always co-expressed with the complementary proteins TTC7B and EFR3B (Chung et al., 2015). Notably, overexpressing Dvl3 increased the plasma membrane component of PIP5KIγ (Fig. 3B) but not of PI4KIIIα (Fig. 3A). Overexpressing PI4KIIIα also increased the plasma membrane component of PIP5KIγ (Fig. 3D), whereas PIP5KIγ only marginally increased the proportion of PI4KIIIα at the plasma membrane (Fig. 3C). Knocking down Dvl3 decreased

Journal of Cell Science (2022) 135, jcs259145. doi:10.1242/jcs.259145

Fig. 3. Dvl3 relocalizes PIP5KIγ to the plasma membrane and promotes colocalization of PI4KIIIα and PIP5KIγ. (A) Left: contrast-inverted confocal micrographs of PI4KIIIα–GFP in tsA-201 cells overexpressing PI4KIIIα–GFP alone (top) or with co-expression of Dvl3–HcRed (bottom). Right: fraction of PI4KIIIα–GFP that distributes to the plasma membrane when the kinase is expressed individually or with Dvl3. Mean±s.e.m. plasma membrane fraction PI4KIIIα–GFP: 0.52±0.03 (*n*=9, PI4KIIIα alone), 0.56±0.02 (*n*=14, PI4KIIIα+Dvl3). For PI4KIIIα, the plasma membrane was delineated by co-expression of CFP–CAAX (pixels positive for CFP–CAAX were used to create a plasma membrane 'mask' to delineate the plasma membrane in the PI4KIIIα–GFP channel). (B) Left: contrast-inverted confocal micrographs of PIP5KIγ–CFP in tsA-201 cells overexpressing PIP5KIγ–CFP alone (top) or with co-expression of Dvl3–HcRed (bottom). Right: mean±s.e.m. plasma membrane fraction of PIP5KIγ–CFP: 0.89±0.02 (*n*=10, PIP5KIγ alone), 0.98±0.01 (*n*=11, PIP5KIγ+Dvl3). (C) Left: contrast-inverted confocal micrographs of PI4KIIIα–GFP in tsA-201 cells overexpressing PI4KIIIα–GFP alone (top) or with co-expression of PIP5KIγ–CFP (bottom). Right: fraction of PI4KIIIα–GFP that distributes to the plasma membrane when expressed alone or with co-expression of PIP5KIγ–CFP. Mean±s.e.m. plasma membrane fraction of PI4KIIIα–GFP: 0.42±0.01 (*n*=20, PI4KIIIα alone), 0.47±0.02 (*n*=31, PI4KIIIα+PIP5KIγ). (D) Left: contrast-inverted confocal micrographs of PIP5KIγ–CFP in tsA-201 cells overexpressing PIP5KIγ–CFP alone (top) or with co-expession of PI4KIIIα–GFP (bottom). Right: fraction of PIP5KIγ–CFP that distributes to the plasma membrane alone or with co-expression of PI4KIIIα–GFP. Mean±s.e.m. plasma membrane fraction PIP5KIγ–CFP: 0.79±0.01 (*n*=13, PIP5KIγ alone), 0.83±0.01 (*n*=31, PIP5KIγ+PI4KIIIα). (E,F) Left: contrast-inverted confocal micrographs of tsA-201 cells overexpressing PI4KIIIα–GFP (E) or PIP5KIγ–CFP (F) alone (top) or with co-expression of siRNA for Dvl3 (siDvl3, bottom). Right: fraction of PI4KIIIα–GFP (E) or PIP5KIγ–CFP (F) that distributes to the plasma membrane alone or with co-expression of siDvl3. CAAX localization was used as a mask to delineate the plasma membrane and as a negative control for the effect of siDvl3. Mean±s.e.m. plasma membrane fraction of PI4KIIIα–GFP (E): 0.59±0.03 (*n*=13, PI4KIIIα alone), 0.64±0.03 (*n*=14, PI4KIIIα+siDvl3). Mean±s.e.m. plasma membrane fraction of PIP5KIγ–CFP (F): 0.84±0.01 (*n*=21, PIP5KIγ alone), 0.78±0.02 (*n*=21, PIP5KIγ+siDvl3). (G) Pearson's coefficient of colocalization derived from confocal micrographs of cells expressing PI4KIIIα–GFP and PIP5KIγ–CFP alone or with co-expression of Dvl3–HcRed or siDvl3. Mean±s.e.m. Pearson's *r* value: 0.27±0.03 (control, *n*=13), 0.37±0.05 (Dvl3, *n*=11), 0.18±0.02 (siDvl3, *n*=12). (H) FRET efficiency between PIP5KIγ–CFP and Dvl3–YFP. Mean±s.e.m. FRET Efficiency: 20.0±3.0% (*n*=25). *P*-values are shown in A–G for the comparisons indicated by horizontal bars (two-tailed unpaired Student's *t*-test in A–D, ANOVA with Dunnett's multiple comparison test in E–G).

the plasma membrane component of PIP5KIγ (Fig. 3F) but had no effect on PI4KIIIα (Fig. 3E). To quantify the magnitude of interaction between overexpressed PI4KIIIα–GFP and PIP5KIγ–CFP, we calculated the Pearson's *r* coefficient from confocal micrographs of control cells, those additionally overexpressing Dvl3, and those with knockdown of Dvl3 using siRNA. Co-expression of Dvl3 increased the Pearson's coefficient (mean Pearson's *r* value=0.37) compared to control cells (mean Pearson's *r* value=0.27), and knocking down Dvl3 reduced colocalization (mean Pearson's *r* value=0.18; Fig. 3G). Measurements of FRET between PIP5KIγ–CFP and Dvl3–YFP support the hypothesis that Dvl3 organizes PIP5KIγ via physical interaction (Fig. 3H).

Dvl3 is necessary for PtdInsP_2 resynthesis

To determine the necessity of Dvl3 for PtdInsP_2 resynthesis, we tested the effects of Dvl3 loss of function on steady-state PtdInsP_2 levels and on the kinetics of PtdInsP_2 resynthesis. An siRNA against Dvl3 (siDvl3) effectively eliminated Dvl3 expression (Fig. 4A). Quantification of PI4KIIIα and PIP5KIγ showed that knocking down Dvl3 had no effect on the endogenous expression of PI4KIIIα or PIP5KIγ (Fig. 4B). Since the voltage activation of KCNQ2/3 channels is strongly sensitive to PtdInsP_2 levels (Kim et al., 2016), we measured the current–voltage relationship in cells with and without expression of siDvl3. With siDvl3, KCNQ2/3 currents required more depolarized potentials to activate, consistent with a decrease in PtdInsP_2 (Fig. 4C). An increase in PtdInsP_2 induced by overexpression of PIP5KIγ had the opposite effect (Fig. 4C), permitting channel opening at less depolarized potentials. Tail currents elicited at a range of voltages were fitted with sigmoid curves yielding a mid-point voltage $V_{1/2}$ of −11.3 mV for control cells, −28.1 mV for cells overexpressing PIP5KIγ and +5.0 mV for cells with siDvl3 (Fig. 4C).

Consistent with a decrease in steady-state plasma membrane PtdInsP_2, siDvl3 reduced the resting fraction of PH-PLCδ1 at the plasma membrane (Fig. 4D). In addition, PH-PLCδ1 returned only partially to the plasma membrane following activation of M_1 receptors (Fig. 4E), indicating a compromised capacity for PtdInsP_2 resynthesis. Treating cells for 15 min with GSK-A1, an inhibitor of PI4KIIIα, elicited a strikingly similar reduction of plasma membrane PtdInsP_2 at rest (Fig. 4F) and impaired resynthesis after receptor activation (Fig. 4G). These data indicate that both PI4KIIIα and Dvl3 are necessary for efficient resynthesis of PtdInsP_2.

Dvl3 and PIP5K move to the plasma membrane in response to Wnt5a

Ror2 is a non-canonical Wnt receptor activated by Wnt5a whose partially characterized downstream signaling includes Dvl proteins. We overexpressed Ror2 receptors and tested whether application of Wnt5a changes the localization of Dvl3 or PIP5KIγ. Using total internal reflection fluorescence (TIRF) microscopy, we found that Wnt5a induced a small and transient translocation of Dvl3 to the plasma membrane, peaking ∼30 s after agonist application and decreasing before agonist was removed (Fig. 5A,B). During this time, the Ror2 receptor remained stable in the plasma membrane. Likewise, confocal microscopy showed a brief recruitment of PIP5KIγ to the plasma membrane, followed by formation of cytosolic bodies labeled for PIP5KIγ (Fig. 5C,D). Thus, addition of Wnt5a to cells overexpressing Ror2 receptors was sufficient to recruit Dvl3 and PIP5KIγ.

Wnt5a increases phosphorylation of Dvl3

We performed immunoblots on cell homogenates from cells overexpressing Ror2 to establish whether Dvl3 is phosphorylated upon application of Wnt5a. Phosphorylation of Dvl proteins is thought to be part of their mechanism of activation (Nishita et al., 2010; Witte et al., 2010). Dvl3 phosphorylation was quantified from immunoblots using an anti-phosphotyrosine antibody, and blot intensity was normalized to control non-stimulated cells (Fig. 5E). We found that stimulation with Wnt5a increased Dvl3 tyrosine phosphorylation, whereas Wnt7a, a canonical agonist that fails to activate Ror2 (Cerpa et al., 2015), had no effect (Fig. 5E).

Ror2 overexpression increases the plasma membrane pool of PtdInsP_2

Overexpressing Ror2 receptors accelerated activation gating of KCNQ2/3 current (Fig. 5F) and slowed down the deactivation of the channel, consistent with an increase in resting plasma membrane PtdInsP_2. Ror2 receptor overexpression also blunted the translocation of PH-PLCδ1 to the cytosol in response to M_1 receptor activation (Fig. 5G), reflective of increased PtdInsP_2 at the plasma membrane and/or accelerated PtdInsP_2 resynthesis. Interestingly, the recovery of PH-PLCδ1 to the plasma membrane appears to be biphasic when Ror2 receptor is overexpressed (Fig. 5G). Confocal micrographs of PH-PLCδ1 taken in the same period show rod-shaped regions adjacent to the plasma membrane (denoted with red

Journal of Cell Science (2022) 135, jcs259145. doi:10.1242/jcs.259145

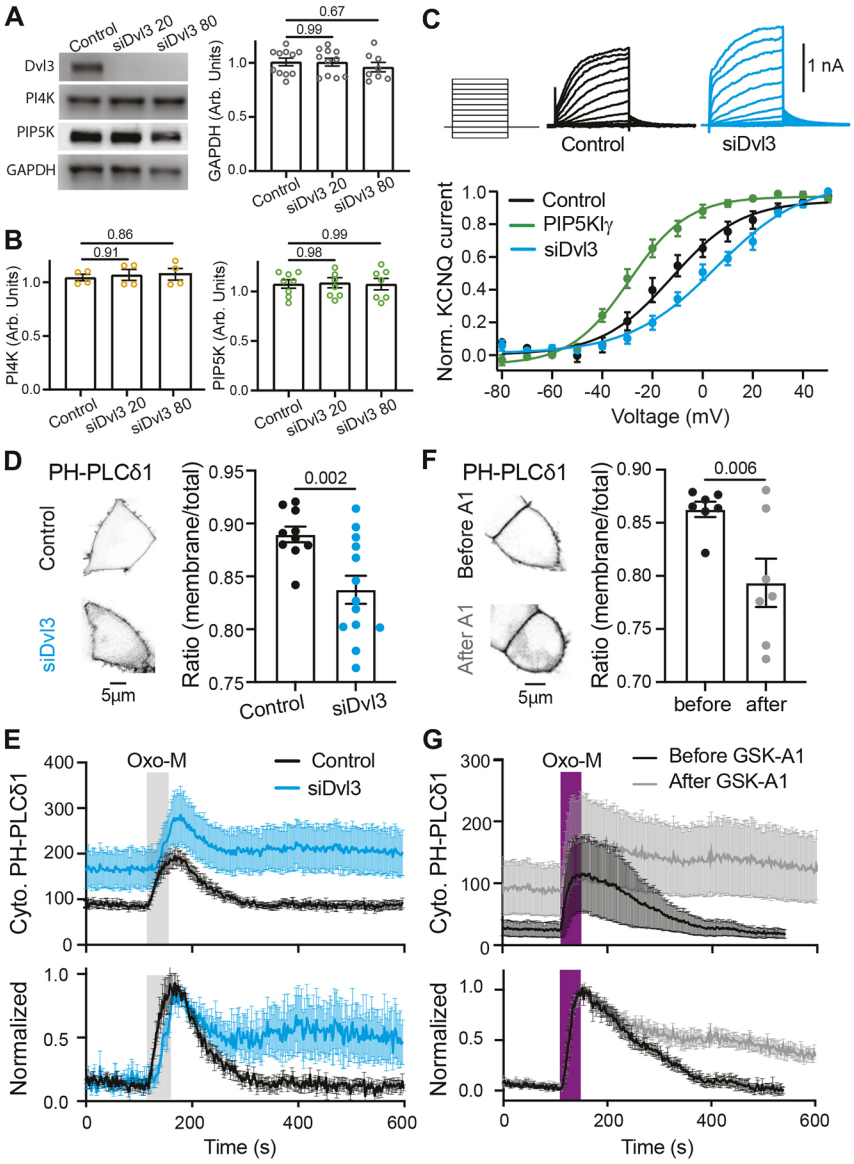

Fig. 4. Downregulation of Dvl3 reduces plasma membrane pools of PtdInsP_2 and prevents a full recovery. (A) Left: immunoblot showing expression of endogenous Dvl3, PI4KIIIα, PIP5KIγ and GAPDH in tsA-201 cells transfected with two different concentrations of siRNA (second column, 20 pmol siDvl3; third column, 80 pmol siDvl3) for Dvl3. Right: quantification of expression of GAPDH. Data are presented as mean ±s.e.m. of 11 experiments. (B) Quantification of expression of PI4KIIIα (left, *n*=4) and PIP5KIγ (right, *n*=7) as in A. Data are presented as mean±s.e.m. (C) Top: representative voltage-clamp currents for tsA-201 cells transfected with KCNQ2 and KCNQ3 (control, black) and those with siRNA against Dvl3 (siDvl3, blue). Bottom: normalized tail current–voltage relationship for cells as in B, and for those overexpressing PIP5KIγ–CFP (green). Mean±s.e.m. half-maximal voltage: −11.3±4.0 mV (*n*=12, control), −28.1±3.0 mV (*n*=7, PIP5KIγ), +5.0±3.9 mV (*n*=6, siDvl3). (D) Left: contrast-inverted confocal micrographs of PH-PLCδ1–YFP in tsA-201 cells expressing PH-PLCδ1–YFP alone (control) or with overexpression of siDvl3. TYE 563 dye fluorescence was used to confirm siDvl3 transfection. Right: membrane fraction of PH-PLCδ1–YFP alone or with co-expression of siDvl3. Mean±s.e.m. plasma membrane fraction PH-PLCδ1: 0.89±0.007 (*n*=10, control), 0.83±0.132 (*n*=13, siDvl3). (E) Time course of cytosolic PH-PLCδ1 alone (control, black) or with overexpression of siRNA for Dvl3 (siDvl3, blue). Oxo-M treatment (1 µM) is indicated by the gray bar. Data are presented as mean±s.e.m. of *n*=6 (control) and *n*=6 (siDvl3). (F) Contrast-inverted confocal micrographs of tsA-201 cells expressing PH-PLCδ1–YFP before and after treatment with PI4KIIIa inhibitor GSK-A1 (100 nM for 15 min) with a graph showing the fraction of PH probe residing in the membrane. Mean±s.e.m. plasma membrane fraction PH-PLCδ1: before GSK-A1 treatment, 0.86±0.007 (*n*=7); after GSK-A1 treatment, 0.79±0.022 (*n*=7). (G) Time course of cytosolic PH-PLCδ1 in control cells before (black) or after (gray) treatment with GSK-A1. Oxo-M treatment (1 µM) is indicated by the magenta bar. Data are presented as mean±s.e.m. of *n*=6 (before GSK-A1) and *n*=6 (after GSK-A1). *P*-values are shown in A,B,D and F for the comparisons indicated by horizontal bars (ANOVA with Dunnett's multiple comparison test in A,B; two-tailed unpaired Student's *t*-test in D,F).

arrows in Fig. 5G). It will be interesting to see whether these possibly intracellular pools of PtdInsP_2 contribute to the slow, second phase of plasma membrane PtdInsP_2 recovery in these cells. This experiment was repeated with Tubby$_C^{R332H}$, another optical probe for PtdInsP_2. Similar kinetics for PtdInsP_2 depletion and recovery upon M_1 receptor activation were observed (Fig. 5H). Even in the absence of exogenous agonist, Ror2 overexpression seems to increase the plasma membrane pool of PtdInsP_2.

Total PtdIns*P* declines in cells overexpressing PI4KIIIα

We conclude with a quantitative assay for phosphoinositides. Mass spectrometry was used to measure levels of PtdIns*P*, PtdInsP_2, and PtdInsP_3. The conditions of transient transfection matched those for which protein expression was detected in Fig. 1B. In cell populations overexpressing PIP5KIγ, we found as expected that PtdIns*P*, the substrate of the PIP5K, declined by 29% and PtdInsP_2, the product, increased by 41% compared to levels in control cells. However, we were surprised to find that overexpression of PI4KIIIα reduced the prevalence of its immediate product, PtdIns*P*, by 22% while still increasing PtdInsP_2 by 29% (Fig. 6A,B). What could account for the diminution of PtdIns*P* when PI4K is overexpressed? We hypothesize that an interaction with PI4KIIIα increased the enzymatic activity of PIP5K. Efficient phosphorylation, without the accumulation of intermediate PtdIns*P*, could be accomplished by coupling of PI4K and PIP5K. PIP5KIγ also increases the prevalence of PtdInsP_3 by 54% (Fig. 6C).

Dvl3 decreases PtdIns*P* and increases PtdInsP_2 and PtdInsP_3

We repeated these mass spectrometry measurements in cells overexpressing Dvl3 and found a 27% decrease in PtdIns*P* (Fig. 6D), a 21% increase in PtdInsP_2 (Fig. 6E) and a 66% increase in PtdInsP_3 (Fig. 6F). For all three phosphoinositides, overexpression of Dvl3 reproduced the effect of overexpressing PI4KIIIα or PIP5KIγ. Dvl3 seems able to mobilize endogenous PI4K and PIP5K in a manner similar to overexpression of those kinases. Given the increase in PtdInsP_3, it could be worth investigating whether the activity of phosphatidylinositol 3-kinases also depends on Dvl3. Our functional and quantitative assays show that Dvl3 increases baseline PtdInsP_2, is required for efficient synthesis of PtdInsP_2, localizes PIP5KIγ to the plasma membrane and promotes colocalization of PI4KIIIα and PIP5KIγ.

Journal of Cell Science (2022) 135, jcs259145. doi:10.1242/jcs.259145

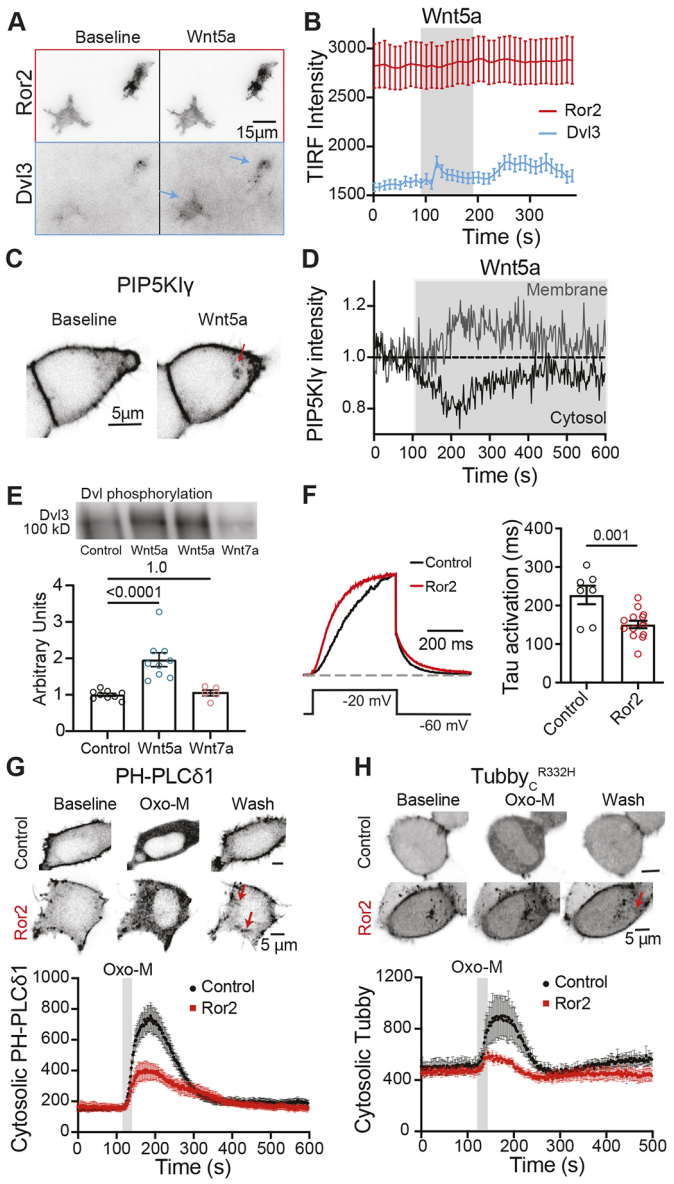

Fig. 5. Wnt5a recruits Dvl3 and PIP5KIγ to the plasma membrane in cells overexpressing Ror2, and Ror2 overexpression increases PtdInsP_2. (A) Contrast-inverted TIRF micrographs of two tsA-201cells overexpressing Ror2–CFP and Dvl3–dsRed at rest (baseline) and in the presence of 125 ng/ml Wnt5a. Under baseline conditions, Dvl3 is minimally present within the evanescent field. After Wnt5a application, Dvl3 appears, and puncta are visible (blue arrows). (B) Time course of Ror2–CFP and Dvl3–dsRed intensity as in A. Addition of Wnt5a is marked by the gray bar. Data are mean±s.e.m. of nine cells. (C) Contrast-inverted confocal micrographs of PIP5KIγ–GFP in tsA-201 cells overexpressing Ror2–mCherry and PIP5KIγ–GFP before and after application of 125 ng/ml Wnt5a. Red arrow indicates intracellular regions containing PIP5KIγ. Images are representative of five cells. (D) Time course of normalized intensity of PIP5KIγ–GFP in the plasma membrane and the cytosol. Application of Wnt5a is indicated by the gray box. Data are representative of five cells. (E) Top: immunoblot showing phosphorylation of Dvl3 without agonist (control) or with exposure to 125 ng/ml Wnt5a or Wnt7a. Bottom: quantification of phosphorylated Dvl3. Mean±s.e.m. Dvl3 phosphorylation (arbitrary units) control, 1.00±0.04 (*n*=9); Wnt5a, 1.96±0.20 (*n*=9); Wnt7a, 1.05±0.08 (*n*=5). (F) Left: representative voltage-clamp current traces from tsA-201 cells overexpressing KCNQ2 and KCNQ3 channel subunits alone (black) or with Ror2–mCherry (red). Current traces were fitted with single exponentials to determine the time constants (tau) of activation and deactivation (right). Mean ±s.e.m. tau activation: control, 220±24 ms (*n*=7); Ror2, 151±10 ms (*n*=14). (G,H) Contrast-inverted confocal micrographs (above) and time courses (below) of cytosolic intensity of PtdInsP_2 probes PH-PLCδ1–YFP (G) or Tubby$_C^{R332H}$–YFP (H) in tsA-201 cells overexpressing M_1 receptor and PtdInsP_2 probes alone (control, black) or with overexpression of Ror2 (red). Red arrows indicate intracellular regions containing PtdInsP_2. Oxo-M treatment is indicated by gray bars in the time courses. Wash, steady state after removal of Oxo-M. Data are mean±s.e.m. of six cells. *P*-values are shown in E and F for the comparisons indicated by horizontal bars (ANOVA with Dunnett's multiple comparison test in E; two-tailed unpaired Student's *t*-test in F).

DISCUSSION

This report shows that PI4K and PIP5K act in coordination to synthesize PtdInsP_2, and that the Dishevelled protein Dvl3 is necessary to organize the two kinases for this task (Fig. 1A). This coordination is important both for maintenance of basal levels of PtdInsP_2 and for replacement of PtdInsP_2 following receptor-induced depletion.

Dvl3 organizes the synergistic activity of PI4KIIIα and PIP5KIγ. Overexpression of Dvl3 in the presence of endogenous phosphoinositide kinases was sufficient to reproduce the changes in PtdInsP_2 observed upon simultaneous overexpression of PI4KIIIα and PIP5KIγ. Dvl3 overexpression recapitulated the increase in resting PtdInsP_2 (Figs 1,6) and acceleration of PtdInsP_2 resynthesis (Fig. 2) present with overexpression of PI4KIIIα and PIP5KIγ. By simply organizing the low-abundance endogenous kinases, Dvl3 is sufficient to increase their efficacy substantially. Indeed, when endogenous Dvl3 was knocked down, resting plasma membrane PtdInsP_2 was reduced and recovery from receptor-induced PtdInsP_2 hydrolysis was incomplete (Fig. 4). Blocking PI4KIIIα in control cells had a markedly similar effect on both resting PtdInsP_2 and PtdInsP_2 resynthesis (Fig. 4G) as Dvl3 knockdown, underscoring both the importance of Dvl and the notion that PI4K is rate limiting in these cells.

Although previous studies have suggested that PI4K is rate limiting for resynthesis of PtdInsP_2 (Falkenburger et al., 2010; Myeong et al., 2020), we provide new details about the specific roles of two kinases. In cells overexpressing PIP5KIγ (but not PI4KIIIα), the translocation of PH-PLCδ1 in response to PLCβ activation is smaller and slower than in control cells. This is presumably because PIP5KIγ continues to generate PtdInsP_2 from PtdIns$P$, counteracting the ongoing PtdInsP_2 hydrolysis and slowing down release of PH-PLCδ1 from the plasma membrane. However, PtdIns$P$ is eventually depleted and becomes rate limiting during PtdInsP_2 resynthesis, as evidenced by PI4KIIIα overexpression advancing the start of PtdInsP_2 resynthesis by 10 s relative to that in control cells (Fig. 2F, orange trace versus black trace after Oxo-M). PIP5KIγ appears to be rate limiting for PtdInsP_2 synthesis during PLCβ activation, and PI4KIIIα is rate limiting for PtdInsP_2 resynthesis after agonist withdrawal. Interestingly, once begun, the rate of resynthesis is similar among control cells and those overexpressing either PI4KIIIα or PIP5KIγ.

What evidence do we have that PI4KIIIα, PIP5KIγ and Dvl3 associate in a physical complex? First, both Dvl3 and PI4KIIIα increase the presence of PIP5KIγ at the plasma membrane (Fig. 3). Second, overexpressing Dvl3 increases colocalization of PI4KIIIα and PIP5KIγ, whereas knocking down Dvl3 decreases PI4K–PIP5K colocalization (Fig. 3G). Third, FRET between PIP5KIγ and Dvl3 shows proximity at a molecular level between these proteins (Fig. 3H). Future biochemical and structural experiments will be important in clarifying how these proteins interact.

Journal of Cell Science (2022) 135, jcs259145. doi:10.1242/jcs.259145

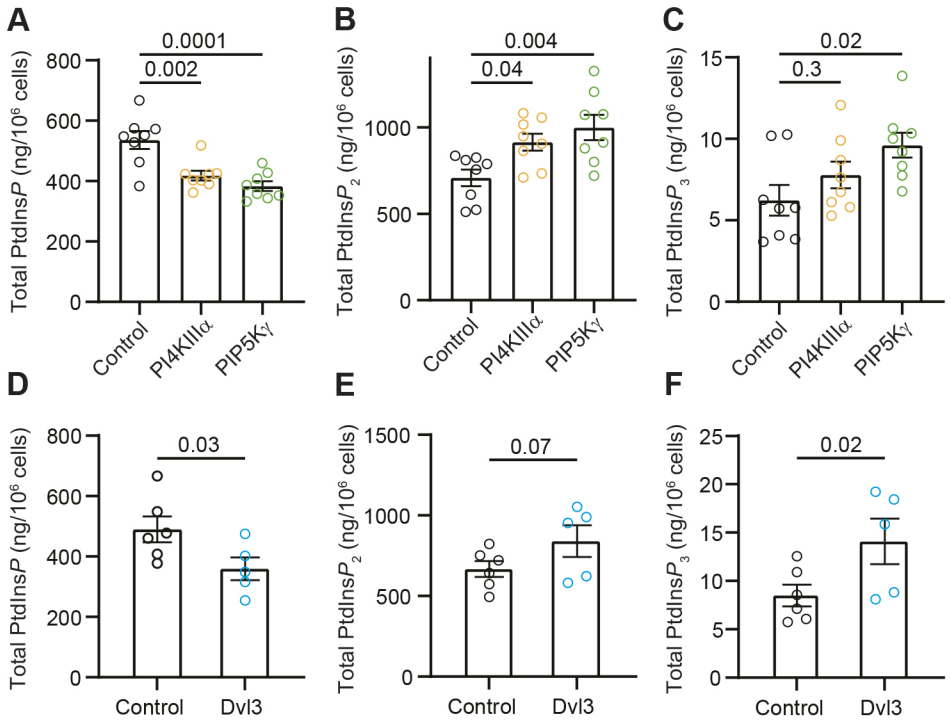

Fig. 6. Overexpression of PI4KIIIα, PIP5Kγ or Dvl3 increases PtdInsP_2. (A) Total PtdIns*P* as measured by mass spectrometry experiments with control tsA201 cells (black), and cells overexpressing PI4KIIIα (orange) or PIP5Kγ (green). Mean±s.e.m. PtdIns*P*: control, 536±30 ng/million cells; PI4KIIIα, 418±16 ng/million cells; PIP5Kγ, 383±16 ng/million cells; *n*=8 dishes. (B) Total PtdInsP_2 as measured by mass spectrometry with cells as in A. Mean±s.e.m. PtdInsP_2: control, 708±48 ng/million cells; PI4KIIIα, 914±49 ng/million cells; PIP5Kγ, 998±73 ng/million cells; *n*=8 dishes. (C) Total PtdInsP_3 as measured by mass spectrometry with cells as in A. Mean±s.e.m. PtdInsP_3: control, 6.3±0.9 ng/million cells; PI4KIIIα, 7.9±0.8 ng/million cells; PIP5Kγ, 9.7±0.8 ng/million cells; *n*=8 dishes. Data in A–C summarize three experiments, two performed in triplicate and one in duplicate. (D) Total PtdIns*P* as measured by mass spectrometry experiments with control tsA201 cells (black), and cells overexpressing Dvl3 (blue). Mean±s.e.m. PtdIns*P*: control, 489±43 ng/million cells (*n*=6 dishes); Dvl3, 359±38 ng/million cells (*n*=5 dishes). (E) Total PtdInsP_2 as measured by mass spectrometry with cells as in D. Mean±s.e.m. PtdInsP_2: control, 668±49 ng/million cells (*n*=6 dishes); Dvl3, 840±99 ng/million cells (*n*=5 dishes). (F) Total PtdInsP_3 as measured by mass spectrometry with cells as in D. Mean±s.e.m. PtdInsP_3: control, 8.5±1.1 ng/million cells (*n*=6 dishes); Dvl3, 14.1±2.4 ng/million cells (*n*=5 dishes). Data in D–F summarize two experiments, one performed in triplicate and one in duplicate. *P*-values are shown for the comparisons indicated by horizontal bars (ANOVA with Dunnett's multiple comparison test).

Following application of Wnt5a in cells overexpressing Ror2, we observed sequential and transient recruitment of Dvl3 and PIP5KIγ to the plasma membrane and increased phosphorylation of Dvl3 (Fig. 5A–E). In addition, Ror2 overexpression increases basal PtdInsP_2 and blunts the translocation of PH-PLCδ1 (Fig. 5G) comparably to overexpression of PIP5KIγ (compare Fig. 1C, Fig. 2D–H). These effects may be due to Ror2 interacting with Dvl3 and recruiting PI4K and PIP5K to the plasma membrane. It will be interesting to investigate these signaling events in neurons, where the depolarization and Ca^{2+} concentration increase downstream of Wnt5a appear to depend on Gαq and PLC (McQuate et al., 2017). For instance, does Ror2 coordinate PI4K and PIP5K activity in hippocampal neurons, and how does that impact events downstream of PLC? Ror2 signaling appears to be context specific depending on co-receptors and accessory proteins (Green et al., 2014), so signaling pathways may vary depending on cell type and receptor expression.

In conclusion, we have shown that Dvl3 organizes PI4KIIIα and PIP5KIγ to synthesize PtdInsP_2 efficiently, especially in response to receptor-induced PtdInsP_2 depletion. Ror2 overexpression increases plasma membrane PtdInsP_2, and Wnt5a stimulates Dvl3 phosphorylation and plasma membrane recruitment of Dvl3 and PIP5KIγ. It will be interesting to determine whether kinase organization plays a role in the etiology of Robinow syndrome arising from mutations in Dvl3.

MATERIALS AND METHODS

Materials

Oxotremorine-M (Oxo-M), GSK-A1, sodium formate, HCl and trimethylsilyl-diazomethane (TMS-DM; 2.0 M in diethyl ether or hexanes) were from Sigma-Aldrich, and Wnt5a was from BD Biosciences. Mass spectrometry-grade methanol, chloroform, dichloromethane and acetonitrile were from Fisher Scientific.

Cell culture and transfection

Cells of the tsA-201 cell line (RRID:CVCL_2737, Sigma-Aldrich), originally derived from HEK-293 human embryonic kidney cells and certified by the vendor by short tandem repeat profiling, were cultivated in DMEM (Fisher Scientific) with 10% fetal bovine serum (Sigma-Aldrich) and 2% penicillin-streptomycin (Gibco), and were used between passages 15 and 50. Cells were transfected at 75–85% confluency using Lipofectamine 2000 or 3000 (Invitrogen) with the following cDNA plasmids: Ror2–mCherry (Cerpa et al., 2015); PI4KIIIa–GFP, EFR3B and TTC7B (from Pietro de Camilli, Yale University, USA); human EGFP–PIP5KIγ_i2 and CFP–PIP5KIγ_i2 (from Rosa Ana Lacalle and Santos Mañes, Centro Nacional de Biotecnología/Consejo Superior de Investigaciones Científicas, Madrid, Spain; Lacalle et al., 2015); human Dvl3–EYFP and Dvl3–HcRed (from Randall Moon, University of Washington, USA); mouse M1 muscarinic receptor (from Neil Nathanson, University of Washington, USA); human eCFP–PH-PLCδ1, eYFP–PH-PLCδ1 and CFP–CAAX (from Kees Jalink, the Netherlands Cancer Institute, Amsterdam, The Netherlands); RFP–PH-PLCδ (from Ken Mackie, Indiana University, USA), Tubby$_C^{R332H}$–YFP (from Andrew Tinker, University College

Journal of Cell Science (2022) 135, jcs259145. doi:10.1242/jcs.259145

London, UK); human KCNQ2 and rat KCNQ3 (from David McKinnon, SUNY Stony Brook, USA); and siRNA for Dvl3 (Santa Cruz Biotechnology). TYE 563 dye (Integrated DNA Technologies) was included with siRNA transfection to screen for successfully transfected cells.

Mass spectrometry

Mass spectrometry was performed as previously described (de la Cruz et al., 2020). In brief, lipids were precipitated from pelleted cells treated with trichloroacetic acid and extracted with chloroform–methanol. Dried extracts were methylated with TMS-DM and quantified by targeted analysis as described previously (Traynor-Kaplan et al., 2017). For each phosphoinositide type, peaks were analyzed for the three most predominant species: 38:4, 36:2 and 36:1. Peak areas were converted to mg per 10^6 cells as described using 37:4 lipid internal standards (Avanti Lipids) and DNA-per-sample measurements.

Electrophysiology

KCNQ2/3 current was recorded by patch clamp in whole-cell configuration at room temperature with a HEKA EPC 9 amplifier (HEKA Elektronik). The resistance of the borosilicate glass pipettes was 3–5 MΩ. Series resistance was ≤10 MΩ and was compensated ≥70%. The bath solution consisted of 160 mM NaCl, 2.5 mM KCl, 2 mM $CaCl_2$, 1 mM $MgCl_2$, 10 mM HEPES and 8 mM glucose adjusted to pH 7.4 with NaOH. The pipette solution consisted of 175 mM KCl, 5 mM $MgCl_2$, 5 mM HEPES, 0.1 mM BAPTA K_4 (Invitrogen), 3 mM Na_2ATP and 0.1 mM Na_3GTP adjusted to pH 7.4 with KOH.

High-resolution microscopy

Confocal images were obtained with an inverted confocal system (Zeiss LSM 880) run by ZEN black v2.3. A Plan Apochromat 63×/1.40 NA oil immersion objective was used. Fluorescent proteins were excited with three lasers tuned to 405 nm, 458–514 nm and 561 nm. Emission light was detected using an Airyscan 32 GaAsP detector and appropriate emission filter sets. The point spread functions were calculated using ZEN black software using 0.1 µm fluorescent microspheres. After deconvolution, the point spread functions were: 124 nm in *x*–*y* and 216 nm in *z* (for 488 nm excitation); 168 nm in *x*–*y* and 212 nm in *z* (for 594 nm excitation). Temperature inside the microscope housing was 27–30°C. Time series were taken with an interval of 2–5 s. Drug perfusion while imaging used a gravity system set to flow at 2 ml min^{-1}. Images were analyzed with ImageJ (NIH, Bethesda, MD, USA). Colocalization analysis was performed using the Fiji (https://fiji.sc/) plugin Coloc 2 to measure the Pearson correlation coefficient.

TIRF microscopy

TIRF microscopy was performed on cells plated on #0 glass coverslips fitted to a recording chamber. TIRF footprints were acquired using a Nikon Eclipse Ti-E microscope equipped with a 60×/1.25 oil-immersion objective and Photometrics QuantEM EMCCD camera (Nikon). Time-series images were taken every 10 s at 23°C and analyzed with ImageJ.

FRET

Three-cube FRET between transfected CFP- and YFP-tagged fluorescent proteins was performed as described previously (Myeong et al., 2020). Briefly, cells were illuminated with 440 nm and 500 nm excitation light from a TILL monochromator (Polychrome IV). Light passed through a three-color dichroic cube (CFP, YFP, mCherry; 89006bs; Chroma Technology Corp.) and a 60×/1.40 oil-immersion objective. An adjustable viewfinder was used to collect emission light from single cells. Emission bands were detected using a beamsplitter, emission filters ET480/24 (CFP) and ET535/30 (YFP; Chroma Technology Co.), photodiodes and a TILL FDU-2 detection unit. Recordings were controlled by an EPC9 amplifier with Patchmaster 2.35 software (HEKA). Photometeric measurements were taken at 23°C. Data were corrected for background and bleed-through, and FRET efficiency was determined as follows:

$$\mathrm{FRETeff} = \frac{\mathrm{SFRET(DA)} - \mathrm{RD1} \times \mathrm{SCFP(DA)}}{[\mathrm{RA1} \times (\mathrm{SYFP(DA)} - \mathrm{RD2} \times \mathrm{SCFP(DA)}) - 1] \times \frac{\mathrm{EYFP}[440]}{\mathrm{ECFP}[440]}},$$

where RD1, RD2 and RA1 are bleed-through constants measured with single fluorophores; SCFP(DA), SYFP(DA) and SFRET(DA) are intensity measurements with the indicated fluorescent cube; and ECFP and EYFP are molar extinction coefficients (Erickson et al., 2001).

Immunoblotting

Cells were homogenized in 500 µl of lysis buffer [50 mM Tris-HCl (pH 7.4), 150 mM NaCl, 5 mM EDTA, 1 mM EGTA, 0.5% protease inhibitor (Millipore Sigma), 1% Triton X-100 and 1% (w/v) deoxycholate] and centrifuged at 11,200 ***g*** for 10 min. Supernatant was extracted, proteins were quantified using the BCA method, and 20 µg of protein was run on a 7.5% polyacrylamide gel. Proteins were transferred to nitrocellulose membrane, blocked with 5% milk for 2 h, and incubated with the primary antibody: rabbit anti-PI4K antibody (#4902; Cell Signaling Technology), mouse anti-PIP5KIγ antibody (H-9, sc-377061; Santa Cruz Biotechnology) or rabbit anti-Dvl3 antibody (#3218; Cell Signaling Technology) for PI4KIIIA, PIP5KI and Dvl3, respectively.

Samples were incubated in primary antibody (1:5000 dilution) overnight and in secondary antibody (1:10,000 dilution) for 2 h [mouse anti-rabbit IgG–HRP (sc-2357, Santa Cruz Biotechnology) or m-IgGκ BP–HRP (sc-516102, Santa Cruz Biotechnology)]. Antibody complexes were detected by chemiluminescence using SuperSignal West Femto Kit (Thermo Fisher Scientific, USA). Chemiluminescence was captured using C-DiGit® Blot Scanner (LI-COR Biosciences, USA).

Immunoprecipitation assay

Cells from three 35 mm dishes were lysed using 500 µl of lysis buffer and centrifuged at 11,200 ***g*** for 10 min. The supernatant was extracted for immunoprecipitation by incubation with 0.5 µg of the rabbit anti-PI4K antibody (#4902; Cell Signaling Technology) and 20 µl Protein A–Sepharose™ 4B (Invitrogen) at 4°C for 2 h. The immune complexes obtained were precipitated for 1 min at 11,200 ***g*** and washed with 1× phosphate-buffered saline (PBS) three times before being dissolved in 15 µl 6× SDS loading buffer (Thermo Fisher Scientific, USA). The sample was run in denaturing electrophoresis with standard running buffer containing SDS and transferred to nitrocellulose membrane, blocked with 5% milk for 2 h, and incubated with the primary antibody (1:5000, rabbit anti-PI4K; #4902, Cell Signaling Technology) at 4°C overnight. A secondary incubation with m-IgGκ BP–HRP (sc-516102; Santa Cruz Biotechnology) at 1:10,000 was performed, and the antibody complexes were detected by chemiluminescence using SuperSignal West Femto Kit (Thermo Fisher Scientific, USA). Chemiluminescence was captured using a C-DiGit® Blot Scanner (LI-COR Biosciences, USA).

Dvl phosphorylation assay

Immunoprecipitation of cells was performed as above, except that supernatant was extracted by incubation with anti-Dvl3 antibody (1:2000; #3218; Cell Signaling Technology) and membranes were incubated with 1:5000 mouse anti-phosphotyrosine primary antibody (#05-321; EMD Milipore Corp.).

Statistics

Mean values in text and figures are given with s.e.m. calculated using GraphPad Prism. *P*-values were determined using two-tailed unpaired Student's *t*-test to compare two groups or ANOVA with Dunnett's multiple comparisons test for three or more groups.

Acknowledgements

We thank Lea Miller for administrative support, Alexis Traynor-Kaplan for assistance with mass spectrometry experiments, and Bertil Hille for invaluable mentorship, critical discussion and feedback on the manuscript.

Competing interests

The authors declare no competing or financial interests.

Author contributions

Conceptualization: L.d.l.C., O.V., A.B., J.B.J.; Methodology: L.d.l.C., R.R., A.B., J.B.J.; Formal analysis: L.d.l.C., R.R., O.V., J.B.J.; Investigation: L.d.l.C., R.R.,

J.B.J.; Writing - original draft: L.d.l.C., J.B.J.; Writing - review & editing: L.d.l.C., O.V., A.B., J.B.J.; Supervision: O.V., A.B.; Project administration: A.B., J.B.J.; Funding acquisition: O.V., A.B.

Funding
This work was supported by National Institutes of Health grants R37-NS08174 to Bertil Hille and MIRA R35-GM142690 to O.V., and a National Science Foundation grant IOS-1755004 to A.B. Deposited in PMC for release after 12 months.

Data availability
The mass spectrometry dataset is available online: https://doi.org/10.6084/m9.figshare.18739265.

Peer review history
The peer review history is available online at https://journals.biologists.com/jcs/article-lookup/doi/10.1242/jcs.259145.

References

Ahmad-Annuar, A., Ciani, L., Simeonidis, I., Herreros, J., Fredj, N. B., Rosso, S. B., Hall, A., Brickley, S. and Salinas, P. C. (2006). Signaling across the synapse: a role for Wnt and Dishevelled in presynaptic assembly and neurotransmitter release. *J. Cell Biol.* **174**: 127-139. doi:10.1083/jcb.200511054

Balla, T. (2013). Phosphoinositides: tiny lipids with giant impact on cell regulation. *Physiol. Rev.* **93**, 1019-1137. doi:10.1152/physrev.00028.2012

Castro-Piedras, I., Sharma, M., Brelsfoard, J., Vartak, D., Martinez, E. G., Rivera, C., Molehin, D., Bright, R. K., Fokar, M., Guindon, J. et al. (2021). Nuclear Dishevelled targets gene regulatory regions and promotes tumor growth. *EMBO Rep.* **22**, e50600. doi:10.15252/embr.202050600

Cerpa, W., Gambrill, A., Inestrosa, N. C. and Barria, A. (2011). Regulation of NMDA-receptor synaptic transmission by Wnt signaling. *J. Neurosci.* **31**: 9466-9471. doi:10.1523/JNEUROSCI.6311-10.2011

Cerpa, W., Latorre-Esteves, E. and Barria, A. (2015). RoR2 functions as a noncanonical Wnt receptor that regulates NMDAR-mediated synaptic transmission. *Proc. Natl. Acad. Sci. U.S.A.* **112**, 4797-4802. doi:10.1073/pnas.1417053112

Chung, J., Nakatsu, F., Baskin, J. M. and De Camilli, P. (2015). Plasticity of PI4KIIIα interactions at the plasma membrane. *EMBO Rep.* **16**: 312-320. doi:10.15252/embr.201439151

Dai, G., Yu, H., Kruse, M., Traynor-Kaplan, A. and Hille, B. (2016). Osmoregulatory inositol transporter SMIT1 modulates electrical activity by adjusting $PI(4,5)P_2$ levels. *Proc. Natl. Acad. Sci. U.S.A.* **113**, E3290-E3299. doi:10.1073/pnas.1606348113

de la Cruz, L., Traynor-Kaplan, A., Vivas, O., Hille, B. and Jensen, J. B. (2020). Plasma membrane processes are differentially regulated by type I phosphatidylinositol phosphate 5-kinases and RASSF4. *J. Cell Sci.* **133**, jcs233254. doi:10.1242/jcs.233254

Erickson, M. G., Alseikhan, B. A., Peterson, B. Z. and Yue, D. T. (2001). Preassociation of calmodulin with voltage-gated Ca^{2+} channels revealed by FRET in single living cells. *Neuron* **31**: 973-985. doi:10.1016/S0896-6273(01)00438-X

Falkenburger, B. H., Jensen, J. B. and Hille, B. (2010). Kinetics of PIP_2 metabolism and KCNQ2/3 channel regulation studied with a voltage-sensitive phosphatase in living cells. *J. Gen. Physiol.* **135**, 99-114. doi:10.1085/jgp.200910345

Green, J., Nusse, R. and van Amerongen, R. (2014). The role of Ryk and Ror receptor tyrosine kinases in Wnt signal transduction. *Cold Spring Harb Perspect Biol.* **6**, a009175. doi:10.1101/cshperspect.a009175

Hille, B., Dickson, E. J., Kruse, M., Vivas, O. and Suh, B. C. (2015). Phosphoinositides regulate ion channels. *Biochim. Biophys. Acta* **1851**: 844-856.

Horowitz, L. F., Hirdes, W., Suh, B. C., Hilgemann, D. W., Mackie, K. and Hille, B. (2005). Phospholipase C in living cells: activation, inhibition, Ca^{2+} requirement, and regulation of M current. *J. Gen. Physiol.* **126**: 243-262. doi:10.1085/jgp.200509309

Hu, J., Yuan, Q., Kang, X., Qin, Y., Li, L., Ha, Y. and Wu, D. (2015). Resolution of structure of PIP5K1A reveals molecular mechanism for its regulation by dimerization and dishevelled. *Nat. Commun.* **6**: 8205. doi:10.1038/ncomms9205

Kim, K. S., Duignan, K. M., Hawryluk, J. M., Soh, H. and Tzingounis, A. V. (2016). The voltage activation of cortical KCNQ channels depends on global PIP2 levels. *Biophys. J.* **110**: 1089-1098. doi:10.1016/j.bpj.2016.01.006

Lacalle, R. A., de Karam, J. C., Martinez-Munoz, L., Artetxe, I., Peregil, R. M., Sot, J., Rojas, A. M., Goni, F. M., Mellado, M. and Manes, S. (2015). Type I phosphatidylinositol 4-phosphate 5-kinase homo- and heterodimerization determines its membrane localization and activity. *FASEB J.* **29**: 2371-2385. doi:10.1096/fj.14-264606

Lees, J. A., Zhang, Y., Oh, M. S., Schauder, C. M., Yu, X., Baskin, J. M., Dobbs, K., Notarangelo, L. D., De Camilli, P., Walz, T. et al. (2017). Architecture of the human PI4KIIIα lipid kinase complex. *Proc. Natl. Acad. Sci. U.S.A.* **114**: 13720-13725. doi:10.1073/pnas.1718471115

Li, Y., Gamper, N., Hilgemann, D. W. and Shapiro, M. S. (2005). Regulation of Kv7 (KCNQ) K^+ channel open probability by phosphatidylinositol 4,5-bisphosphate. *J. Neurosci.* **25**: 9825-9835. doi:10.1523/JNEUROSCI.2597-05.2005

Mandal, K. (2020). Review of PIP2 in cellular signaling, functions and diseases. *Int. J. Mol. Sci.* **21**, 8342. doi:10.3390/ijms21218342

McQuate, A., Latorre-Esteves, E. and Barria, A. (2017). A Wnt/Calcium signaling cascade regulates neuronal excitability and trafficking of NMDARs. *Cell Rep.* **21**, 60-69. doi:10.1016/j.celrep.2017.09.023

Myeong, J., de la Cruz, L., Jung, S. R., Yeon, J. H., Suh, B. C., Koh, D. S. and Hille, B. (2020). Phosphatidylinositol 4,5-bisphosphate is regenerated by speeding of the PI 4-kinase pathway during long PLC activation. *J. Gen. Physiol.* **152**, e202012627. doi:10.1085/jgp.202012627

Nakatsu, F., Baskin, J. M., Chung, J., Tanner, L. B., Shui, G., Lee, S. Y., Pirruccello, M., Hao, M., Ingolia, N. T., Wenk, M. R. et al. (2012). PtdIns4P synthesis by PI4KIIIα at the plasma membrane and its impact on plasma membrane identity. *J. Cell Biol.* **199**: 1003-1016. doi:10.1083/jcb.201206095

Nishita, M., Itsukushima, S., Nomachi, A., Endo, M., Wang, Z., Inaba, D., Qiao, S., Takada, S., Kikuchi, A. and Minami, Y. (2010). Ror2/frizzled complex mediates Wnt5a-induced AP-1 activation by regulating dishevelled polymerization. *Mol. Cell. Biol.* **30**: 3610-3619. doi:10.1128/MCB.00177-10

Olivença, D. V., Uliyakina, I., Fonseca, L. L., Amaral, M. D., Voit, E. O. and Pinto, F. R. (2018). A mathematical model of the phosphoinositide pathway. *Sci. Rep.* **8**: 3904. doi:10.1038/s41598-018-22226-8

Qin, Y., Li, L., Pan, W. and Wu, D. (2009). Regulation of phosphatidylinositol kinases and metabolism by Wnt3a and Dvl. *J. Biol. Chem.* **284**: 22544-22548. doi:10.1074/jbc.M109.014399

Sharma, M., Castro-Piedras, I., Simmons, G. E., Jr. and Pruitt, K. (2018). Dishevelled: A masterful conductor of complex Wnt signals. *Cell. Signal.* **47**: 52-64. doi:10.1016/j.cellsig.2018.03.004

Sheldahl, L. C., Slusarski, D. C., Pandur, P., Miller, J. R., Kuhl, M. and Moon, R. T. (2003). Dishevelled activates Ca^{2+} flux, PKC, and CamKII in vertebrate embryos. *J. Cell Biol.* **161**: 769-777.

Traynor-Kaplan, A., Kruse, M., Dickson, E. J., Dai, G., Vivas, O., Yu, H., Whittington, D. and Hille, B. (2017). Fatty-acyl chain profiles of cellular phosphoinositides. *Biochim Biophys Acta Mol Cell Biol Lipids* **1862**: 513-522.

Varnai, P., Thyagarajan, B., Rohacs, T. and Balla, T. (2006). Rapidly inducible changes in phosphatidylinositol 4,5-bisphosphate levels influence multiple regulatory functions of the lipid in intact living cells. *J. Cell Biol.* **175**: 377-382. doi:10.1083/jcb.200607116

White, J., Mazzeu, J. F., Hoischen, A., Jhangiani, S. N., Gambin, T., Alcino, M. C., Penney, S., Saraiva, J. M., Hove, H., Skovby, F. et al. (2015). DVL1 frameshift mutations clustering in the penultimate exon cause autosomal-dominant Robinow syndrome. *Am. J. Hum. Genet.* **96**: 612-622. doi:10.1016/j.ajhg.2015.02.015

White, J. J., Mazzeu, J. F., Hoischen, A., Bayram, Y., Withers, M., Gezdirici, A., Kimonis, V., Steehouwer, M., Jhangiani, S. N., Muzny, D. M. et al. (2016). DVL3 alleles resulting in a -1 frameshift of the last exon mediate autosomal-dominant robinow syndrome. *Am. J. Hum. Genet.* **98**: 553-561. doi:10.1016/j.ajhg.2016.01.005

White, J. J., Mazzeu, J. F., Coban-Akdemir, Z., Bayram, Y., Bahrambeigi, V., Hoischen, A., van Bon, B. W. M., Gezdirici, A., Gulec, E. Y., Ramond, F. et al. (2018). WNT signaling perturbations underlie the genetic heterogeneity of robinow syndrome. *Am. J. Hum. Genet.* **102**: 27-43. doi:10.1016/j.ajhg.2017.10.002

Witte, F., Bernatik, O., Kirchner, K., Masek, J., Mahl, A., Krejci, P., Mundlos, S., Schambony, A., Bryja, V. and Stricker, S. (2010). Negative regulation of Wnt signaling mediated by CK1-phosphorylated Dishevelled via Ror2. *FASEB J.* **24**: 2417-2426. doi:10.1096/fj.09-150615